PERGAMON

Pattern Recognition 35 (2002) 155–167

PATTERN RECOGNITION
THE JOURNAL OF THE PATTERN RECOGNITION SOCIETY

www.elsevier.com/locate/patcog

A geometry-based error estimation for cross-ratios☆

J.-S. Liu, J.-H. Chuang*

Department of Computer and Information Science, National Chiao Tung University, 1001 Ta Hsueh Rd, Hsinchu, Taiwan 30050, ROC

Received 17 March 2000; accepted 19 October 2000

Abstract

For choosing specific cross-ratios as 2D projective coordinates in various computer vision applications, a reasonable error analysis model is usually required. This investigation adopts the assumption of normal distribution for positioning errors of point features in an image to formulate the error variances of cross-ratios. Based on a geometry-based error analysis, a straightforward way of identifying the cross-ratios with minimum error variances is proposed. Simulation results show that the proposed approach, as well as a further simplified alternative, yield much better estimations of minimum error variances in terms of accuracy, cost, and stability compared with some other methods, e.g., the one based on the rule given by Georis et al. (IEEE Trans. Pattern Anal. Mach. Intell. 20 (4) (1998) 366). Some causes of the performance differences in the estimations are explained using a special configuration of point features.

Keywords: Error analysis; Cross-ratio; Computer vision; 3D reconstruction

1. Introduction

Recently, more and more computer vision researchers have been paying attention to error analysis so as to fulfill the accuracy requirements arising from various applications such as outer-space exploration, industrial robots, and so on. In fact, one of the main purposes of computer vision is to construct a reliable system that can carry out its tasks with satisfactory efficiency and precision in a realistic environment. Early works regarding these requirements are mainly concerned with the analysis of error propagation, which are well known in the photogrammetry literature [2–4], and thereby provide relevant information of quality estimation for different steps of a vision algorithm [5]. In particular, such an analysis is often required for 3D shape reconstruction methodologies. There are basically two classes of methods to reconstruct 3D shapes from 2D images. The first class involves strategies relying on camera calibration [6–8] and the second consists of methods based on projective geometry, which usually utilize reference points as prior knowledge [9–13]. Due to the simplicity, some of the projective geometry-based approaches have also been used in other applications [14–17].

Consider the projective geometry-based approaches for 3D reconstruction. In Ref. [9], it is shown that reference points in a sequence of images can be used easily to derive 3D information of objects in a scene. It is also found in Ref. [10] that, given more locations of epipoles, in addition to only four corresponding reference points, a projective invariant structure can be established to reconstruct a 3D scene without any prior knowledge of camera geometry or internal calibration. Subsequently, a relatively affine structure is proposed with one of its applications being the basis for algorithms performing 3D reconstruction from multiple views [11]. Similarly, geometric constructive solutions to 3D vision problems, e.g., positioning a point in the 3D space using two stereo images, are reported in Refs. [12,13].

For the projective geometry-based 3D reconstruction relying on reference points, the quality of the reconstruction strongly depends on that of the image data. In addition to other possible measurement uncertainties,

☆This work was supported by the National Science Council, Republic of China, under grant NSC88-2213-E009-062.

* Corresponding author: Tel.: + 886-3-573-1979; fax: + 886-3-572-1490.

E-mail address: jhchuang@cis.nctu.edu.tw (J.-H. Chuang).

0031-3203/01/$20.00
PII: S0031-3203(00)00174-6

2D coordinates of feature points in an image plane will always have quantization errors due to the limited image resolution. Hence, the projective coordinates, i.e., pairs of cross-ratios with respect to the reference points, will also have error in their values. Such errors must be carefully analyzed and controlled so as not to seriously influence the final reconstruction results.

Several researchers consider the error analysis for cross-ratios obtained for point feature with respect to four reference points [18,19]. The analyses are based on the assumption of an independent, identical, Gaussian distribution of errors in the locations of the four image points in an image plane. A given image of four collinear points is first classified by making comparisons between the measured cross-ratio and those stored in the model database. Subsequently, the performance of the classification is described quantitatively by the probabilities of rejection, false alarm and misclassification. Recently, a complete sensitivity analysis of the 3D reconstruction method based on projective geometry has been presented in Ref. [1] in which the error estimation for the projective coordinates, i.e., cross-ratios, is considered. As one of the main results, it is suggested by the authors that, instead of expensively calculating the error variances of all 24 cross-ratios associated with a 2D feature point, one could choose the cross-ratios which minimize $|\theta - 90^\circ|$.[1] However, such a geometrically phrased criterion is only based on observations on limited number of examples and lacks obvious mathematical support. In this paper, a new approach of estimating error variances of cross-ratios is proposed. It is shown that with a more clear geometric interpretation of the mathematical formulation of the error variances, the proposed approach will perform the error estimation more satisfactorily in terms of accuracy, cost and stability.

The rest of the paper is organized as follows. In Section 2, we give an overview of the projective geometry-based 3D reconstruction. Subsequently, the error generated in the output of the first stage of the reconstruction, i.e., the projective coordinates, due to quantization errors in locations of image points is formulated in Section 3. In Section 4, the geometry-based mathematical reasoning of the above error is carried out and, accordingly, a new error estimation approach is established. Furthermore, by simplifying the estimation process, a low-cost alternative is also introduced. In Section 5, simulations are performed using a typical configuration of a set of four reference points as well as a special configuration wherein three of the four reference points are nearly collinear. Experiments using a real image are also carried out for the latter. Finally, we draw conclusions in Section 6.

[1] Detailed description of the criterion is given in Section 3.

2. Projective geometry-based 3D reconstruction

In this section, we briefly review some mathematics involved in the projective geometry-based 3D reconstruction approach. Let J, K, L and M be four collinear points, as shown in Fig. 1; their cross-ratio is defined as

$$k_1 = [J, K; L, M] = \frac{JL \cdot KM}{KL \cdot JM}, \tag{1}$$

where JL stands for the directed distance from J to L, and so on.[2] In fact, the cross-ratio is the basic invariant in projective geometry: all other projective invariants can be derived from it [20].

Let l_0 denote the line containing the four points with the line equation

$$\mathbf{r} = \mathbf{b} + \mu\mathbf{d}, \tag{2}$$

where $\mathbf{r}$ is the position vector of any point on l_0, $\mathbf{b}$ and $\mathbf{d}$ are the base and directional vectors of the line, respectively, and μ is a parameter taking real values. If μ_J, μ_K, μ_L and μ_M are the μ-parameters associated with J, K, M and L, respectively, the cross-ratio defined in Eq. (1) can also be expressed as

$$k_1 = [J, K; L, M] = \frac{\mu_J - \mu_L}{\mu_K - \mu_L}\frac{\mu_K - \mu_M}{\mu_J - \mu_M}. \tag{3}$$

An immediate application of the invariant property of cross-ratio is to locate a point on a line. For example, assuming that cross-ratio k_1 is given, so are the locations of J, K, L on l_0, it is easy to see from Eq. (3) that the location of M can be determined as

$$\mu_M = \frac{k_1\mu_J(\mu_K - \mu_L) - \mu_K(\mu_J - \mu_L)}{k_1(\mu_K - \mu_L) - (\mu_J - \mu_L)}. \tag{4}$$

Therefore, k_1 can be regarded as the 1D *projective coordinate* of M with respect to $\{J, K, L\}$.

On the other hand, the same idea can be extended to locate a 2D point P_1, also shown in Fig. 1, in a projective plane P^2. This can be done by using two cross-ratios as follows. Assume that points A, B, C and D are given, and so is an arbitrarily chosen line l_0. The location of M, and thus line l_4, can be obtained using Eq. (4) if k_1 is given. Similarly, l_4' can be determined if another cross-ratio, say k_2, is given for the intersections of another arbitrarily chosen l_0' (not shown) and the four lines (including l_4' passing through C). Thus, the location of P_1 can be

[2] Note that the definition of cross-ratio is not unique. Different cross-ratios can be obtained by reordering the four points in Eq. (1). The definitions will give a total of six different cross-ratio values and any one of the values can be used to derive the rest of them [21].

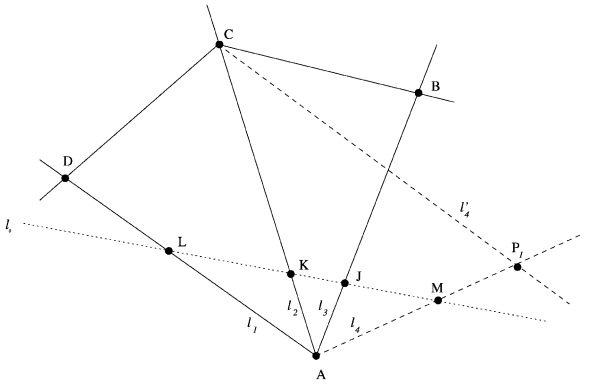

Fig. 1. Definition of cross-ratio and its application in finding 1D (2D) location of point M (P_1).

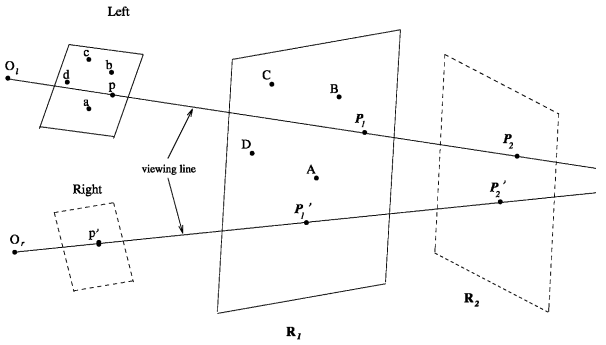

Fig. 2. Reconstruction of a 3D point using projective coordinates.

obtained as the intersection of l_4 and l'_4. Therefore, (k_1, k_2) can be regarded as the 2D *projective coordinates* of P_1 with respect to $\{A, B, C, D\}$.

One main application of the projective coordinates is to reconstruct the world coordinates of a 3D point from its projective images. To see the reconstruction procedure, consider the example shown in Fig. 2. Assume that two reference planes R_1 and R_2 and the 3D locations of four reference points on each of them are given (only A, B, C and D on R_1 are shown). Let p and p' be two images of the feature point P and the two viewing lines intersect R_1 and R_2 at $\{P_1, P_2\}$ and $\{P'_1, P'_2\}$, respectively. Since the projective coordinates of P_1 can be obtained from a, b, c, d and p in the left image plane, the location of P_1 on R_1 and thus its 3D location can be determined. Similarly, the 3D location of P_2, can also be calculated. In the same way, from the right image plane, the 3D locations of P'_1 and P'_2 can also be obtained. Finally, the 3D location of the feature point P in the world coordinates system can be determined as the intersection of the two viewing lines, $\overline{P_1P_2}$ and $\overline{P'_1P'_2}$.

Thus, for a 3D feature point P, the projective geometry-based 3D reconstruction approach using two reference planes can be summarized with the following procedure:

The line intersection (LI) procedure:

Stage 1. Calculate the 2D projective coordinates of P in the left and the right image, respectively, for each reference plane.

Stage 2. Calculate the 3D locations of the two images of P on each reference plane using the 2D projective coordinates computed in Stage 1.

Stage 3. Reconstruct P as the intersection of two viewing lines.

In the above reconstruction procedures, quantization errors in locating point features in the image planes will result in errors in the location of reconstructed object points. However, there will be different error amplification effects on different projective coordinates used in Stage 1 of procedure *LI*. In the next section, an error analysis based on a normal distribution assumption for the above quantization error will be presented.

3. Error analysis

We now present an analysis of the errors in the projective coordinates due to quantization errors in locating point features in 2D images. Such coordinates are useful in projective geometry-based computer vision, e.g., in the reconstruction procedure reviewed in the previous section. Consider the left image shown in Fig. 2. Let j, k, l and m (not shown) be the projective projections of J, K, L and M (see also Fig. 1), respectively. Moreover, let $\mathbf{b}^* + \mu\mathbf{d}^*$ denote the line equation of l_0^* (the image of l_0) for the 2D coordinates system used in that image, where $\mathbf{b}^* = (b_x^*, b_y^*)$ and $\mathbf{d}^* = (d_x^*, d_y^*)$. The intersection of l_0^* and $\overline{ab}$ can be obtained as

$$\mu_j = \frac{a_x b_y - a_y b_x + b_y^* b_x - b_y^* a_x - b_x^* b_y + b_x^* a_y}{d_x^*(b_y - a_y) - d_y^*(b_x - a_x)}, \qquad (5)$$

where (a_x, a_y) and (b_x, b_y) are the coordinates of points a and b, respectively. With similar computations, μ_k, μ_l and μ_m can also be obtained. By using μ_j, μ_k, μ_l and μ_m in place of μ_J, μ_K, μ_L and μ_M, respectively, in Eq. (3), we have

$$k_1 = \frac{(a_x b_y - a_y b_x + b_x d_y - b_y d_x + d_x a_x - d_y a_x)}{(a_x c_y - a_y c_x + c_x d_y - c_y d_x + d_x a_x - d_y a_x)} \times \frac{(a_x c_y - a_y c_x + c_x p_y - c_y p_x + p_x a_y - p_y a_x)}{(a_x b_y - a_y b_x + b_x p_y - b_y p_x + p_x a_y - p_y a_x)}. \qquad (6)$$

Table 1
Cross-ratios associated with a point p and four reference points $\{a, b, c, d\}$

i	Cross-ratio k_i	Dep.	i	Cross-ratio k_i	Dep.
1	$[ab, ac, ad, ap] = \frac{\triangle(a,b,d)\triangle(a,c,p)}{\triangle(a,c,d)\triangle(a,b,p)}$	t_1	13	$[cb, ca, cd, cp] = \frac{\triangle(c,b,d)\triangle(c,a,p)}{\triangle(c,a,d)\triangle(c,b,p)}$	$\frac{t_1}{t_2}$
2	$[ab, ad, ac, ap] = \frac{\triangle(a,b,c)\triangle(a,d,p)}{\triangle(a,d,c)\triangle(a,b,p)}$	$1 - t_1$	14	$[cb, cd, ca, cp] = \frac{\triangle(c,b,a)\triangle(c,d,p)}{\triangle(c,d,a)\triangle(c,b,p)}$	$\frac{t_2 - t_1}{t_2}$
3	$[ac, ab, ad, ap] = \frac{\triangle(a,c,d)\triangle(a,b,p)}{\triangle(a,b,d)\triangle(a,c,p)}$	$\frac{1}{t_1}$	15	$[ca, cb, cd, cp] = \frac{\triangle(c,a,d)\triangle(c,b,p)}{\triangle(c,b,d)\triangle(c,a,p)}$	$\frac{t_2}{t_1}$
4	$[ac, ad, ab, ap] = \frac{\triangle(a,c,b)\triangle(a,d,p)}{\triangle(a,d,b)\triangle(a,c,p)}$	$\frac{t_1 - 1}{t_1}$	16	$[ca, cd, cb, cp] = \frac{\triangle(c,a,b)\triangle(c,d,p)}{\triangle(c,d,b)\triangle(c,a,p)}$	$\frac{t_1 - t_2}{t_1}$
5	$[ad, ac, ab, ap] = \frac{\triangle(a,d,b)\triangle(a,c,p)}{\triangle(a,c,b)\triangle(a,d,p)}$	$\frac{t_1}{t_1 - 1}$	17	$[cd, ca, cb, cp] = \frac{\triangle(c,d,b)\triangle(c,a,p)}{\triangle(c,a,b)\triangle(c,d,p)}$	$\frac{t_1}{t_1 - t_2}$
6	$[ad, ab, ac, ap] = \frac{\triangle(a,d,c)\triangle(a,b,p)}{\triangle(a,b,c)\triangle(a,d,p)}$	$\frac{1}{1 - t_1}$	18	$[cd, cb, ca, cp] = \frac{\triangle(c,d,a)\triangle(c,b,p)}{\triangle(c,b,a)\triangle(c,d,p)}$	$\frac{t_2}{t_2 - t_1}$
7	$[ba, bc, bd, bp] = \frac{\triangle(b,a,d)\triangle(b,c,p)}{\triangle(b,c,d)\triangle(b,a,p)}$	t_2	19	$[db, dc, da, dp] = \frac{\triangle(d,b,a)\triangle(d,c,p)}{\triangle(d,c,a)\triangle(d,b,p)}$	$\frac{t_1 - t_1}{t_2 - 1}$
8	$[ba, bd, bc, bp] = \frac{\triangle(b,a,c)\triangle(b,d,p)}{\triangle(b,d,c)\triangle(b,a,p)}$	$1 - t_2$	20	$[db, da, dc, dp] = \frac{\triangle(d,b,c)\triangle(d,a,p)}{\triangle(d,a,c)\triangle(d,b,p)}$	$\frac{t_1 - 1}{t_2 - 1}$
9	$[bc, ba, bd, bp] = \frac{\triangle(b,c,d)\triangle(b,a,p)}{\triangle(b,a,d)\triangle(b,c,p)}$	$\frac{1}{t_2}$	21	$[dc, db, da, dp] = \frac{\triangle(d,c,a)\triangle(d,b,p)}{\triangle(d,b,a)\triangle(d,c,p)}$	$\frac{t_2 - 1}{t_2 - t_1}$
10	$[bc, bd, ba, bp] = \frac{\triangle(b,c,a)\triangle(b,d,p)}{\triangle(b,d,a)\triangle(b,c,p)}$	$\frac{t_2 - 1}{t_2}$	22	$[dc, da, db, dp] = \frac{\triangle(d,c,b)\triangle(d,a,p)}{\triangle(d,a,b)\triangle(d,c,p)}$	$\frac{t_1 - 1}{t_1 - t_2}$
11	$[bd, bc, ba, bp] = \frac{\triangle(b,d,a)\triangle(b,c,p)}{\triangle(b,c,a)\triangle(b,d,p)}$	$\frac{t_2}{t_2 - 1}$	23	$[da, dc, db, dp] = \frac{\triangle(d,a,b)\triangle(d,c,p)}{\triangle(d,c,b)\triangle(d,a,p)}$	$\frac{t_1 - t_2}{t_1 - 1}$
12	$[bd, ba, bc, bp] = \frac{\triangle(b,d,c)\triangle(b,a,p)}{\triangle(b,a,c)\triangle(b,d,p)}$	$\frac{1}{1 - t_2}$	24	$[da, db, dc, dp] = \frac{\triangle(d,a,c)\triangle(d,b,p)}{\triangle(d,b,c)\triangle(d,a,p)}$	$\frac{t_2 - 1}{t_1 - 1}$

To give a geometric interpretation to the above equation, define the triangle function

$$\triangle(A,B,C) \triangleq \tfrac{1}{2}(A_xB_y - A_yB_x + B_xC_y - B_yC_x + C_xA_y - C_yA_x), \quad (7)$$

whose magnitude, $|\triangle(A,B,C)|$, gives the area of triangle $\triangle ABC$.[3] With this definition, we can rewrite Eq. (6) as

$$k_1 = \frac{\triangle(a,b,d)\,\triangle(a,c,p)}{\triangle(a,c,d)\,\triangle(a,b,p)}. \quad (8)$$

Since six different cross-ratios can be obtained for each of the four reference points being the origin of the pencil of the reference lines going through (i) the other three reference points and (ii) the measured point p, a total of 24 different cross-ratios k_i $1 \leqslant i \leqslant 24$ can be used for p, as listed in Table 1.[4] In theory, if the projective coordinates, as well as other relevant quantities, are calculated precisely, 3D object points can be reconstructed perfectly with procedure *LI*. However, quantization errors are intrinsic to locations of point features extracted from an image, which will result in errors in the computation of projective coordinates as well as in the reconstruction. Often, the normal distribution is utilized to model such quantization errors, which is usually assumed to have a zero mean and the following covariance matrix:

$$\begin{pmatrix} \sigma_{xx}^2 & \sigma_{xy} \\ \sigma_{xy} & \sigma_{yy}^2 \end{pmatrix}.$$

[3] In particular, we have $\triangle(A,B,C) = \triangle(B,C,A) = \triangle(C,A,B) = -\triangle(A,C,B) = -\triangle(C,B,A) = -\triangle(B,A,C)$.

[4] In this table, *Dep.* indicates the dependency between the twenty four definitions of cross-ratio; for example, if k_1 is represented by t_1, then k_2 can be obtained by $1 - t_1$.

Accordingly, the variance of cross-ratio k_1, for example, can be calculated as

$$\begin{aligned}\sigma^2_{k_1,k_1} &= \left[\left(\frac{\partial k_1}{\partial a_x}\right)^2 + \left(\frac{\partial k_1}{\partial b_x}\right)^2 + \left(\frac{\partial k_1}{\partial c_x}\right)^2 + \left(\frac{\partial k_1}{\partial d_x}\right)^2 + \left(\frac{\partial k_1}{\partial p_x}\right)^2\right]\sigma^2_{xx} \\ &+ \left[\left(\frac{\partial k_1}{\partial a_y}\right)^2 + \left(\frac{\partial k_1}{\partial b_y}\right)^2 + \left(\frac{\partial k_1}{\partial c_y}\right)^2 + \left(\frac{\partial k_1}{\partial d_y}\right)^2 + \left(\frac{\partial k_1}{\partial p_y}\right)^2\right]\sigma^2_{yy} \\ &+ 2\left[\frac{\partial k_1}{\partial a_x}\frac{\partial k_1}{\partial a_y} + \frac{\partial k_1}{\partial b_x}\frac{\partial k_1}{\partial b_y} + \frac{\partial k_1}{\partial c_x}\frac{\partial k_1}{\partial c_y} + \frac{\partial k_1}{\partial d_x}\frac{\partial k_1}{\partial d_y} + \frac{\partial k_1}{\partial p_x}\frac{\partial k_1}{\partial p_y}\right]\sigma_{xy} \\ &\triangleq e_{k_1x}\sigma^2_{xx} + e_{k_1y}\sigma^2_{yy} + e_{k_1xy}\sigma_{xy}, \end{aligned} \tag{9}$$

where e_{k_1x}, e_{k_1y}, and e_{k_1xy} are defined as the error amplification factors for σ^2_{xx}, σ^2_{yy}, and σ_{xy}, respectively. Thus, given the repetition/symmetry of Table 1, and the probability that in any practical application all measured points will have equal error, different cross ratios (k_i's) will statistically have different error variances ($\sigma^2_{k_i,k_i}$) according to Eq. (9). Specifically, $\sigma^2_{k_i,k_i}$ is equal to the weighted sum of σ^2_{xx}, σ^2_{yy} and σ_{xy} with the weighting factors equal to non-identical e_{k_ix}, e_{k_iy}, and e_{k_ixy}, respectively. For simplicity, for locating of a point feature in an image, it is assumed that the correlation between the inaccuracies in x and y directions can be ignored, i.e., $\sigma_{xy} \cong 0$. Consequently, only the two amplification factors, e_{k_1x} and e_{k_1y}, will need to be considered in Eq. (9).

Note that, even though the above error analysis is formulated for k_1, a similar analysis for other projective coordinates can also be performed. In general, the amplification factors may vary widely for different cross-ratios being used as projective coordinates, e.g., in Stage 1 of procedure *LI*. In Ref. [1], instead of calculating all the error variances associated with the 24 cross-ratios and then choosing the ones with the smallest variance, it is suggested that cross-ratios which minimize $|\theta - 90^\circ|$ should be used. According to their definition, for each of the 24 cross-ratios listed in Table 1,

$$\theta = \angle o'op,$$

where $o, o' \in \{a, b, c, d\}$, $o \neq o'$, and $\triangle(o, o', p)$ is the second triangle function in the denominator. For example, $\angle CAP_1 = 82.8^\circ$ in Fig. 1 and will minimize $|\theta - 90^\circ|$. Therefore, either k_3 or k_4 shown in Table 1 should be used. However, the authors simply use an example to suggest that a cross-ratio thus obtained is "more likely" to be robust, without giving any obvious mathematical support.

4. Proposed algorithms for error estimation

As noted previously, the calculation for all the amplification factors is time-consuming and a quick estimation of their relative magnitude is usually desired in time-limited situations such as in real-time computer vision, etc. In this section, we will suggest different ways of estimating the minimum error amplification factors based on a geometry-based analysis of Eq. (9). It is shown in Section 5 that the estimation approaches presented in this paper can generate better estimates than the afore mentioned $|\theta - 90^\circ|$ criterion with less computation.

4.1. Definition and a geometry-based error analysis

To estimate the relative magnitude of error amplification factors for different cross-ratios, let us first consider the factor e_{k_1x} in Eq. (9). For the first partial derivative given in Eq. (9), we have

$$\begin{aligned}\frac{\partial k_1}{\partial a_x} &= \frac{(\triangle(a,b,d)\triangle(a,c,p))'\,(\triangle(a,b,p)\triangle(a,c,d)) - (\triangle(a,b,p)\triangle(a,c,d))'(\triangle(a,b,d)\triangle(a,c,p))}{(\triangle(a,b,p)\triangle(a,c,d))^2} \\ &= \frac{[(b_y - d_y)\triangle(a,c,p) + (c_y - p_y)\triangle(a,b,d)]\triangle(a,b,p)\triangle(a,c,d)}{(\triangle(a,b,p)\triangle(a,c,d))^2} \\ &\quad - \frac{[(b_y - p_y)\triangle(a,c,d) + (c_y - d_y)\triangle(a,b,p)]\triangle(a,b,d)\triangle(a,c,p)}{(\triangle(a,b,p)\triangle(a,c,d))^2}. \end{aligned} \tag{10}$$

Similar expressions can be obtained for other partial derivatives. Subsequently, the amplification factor e_{k_1x} in Eq. (9) can be evaluated as

$$\begin{aligned}e_{k_1x} = \frac{1}{[\triangle(a,b,p)\triangle(a,c,d)]^4} &\times \{[[(b_y - d_y)\triangle(a,c,p) + (c_y - p_y)\triangle(a,b,d)] \\ &\times \triangle(a,b,p)\triangle(a,c,d)\end{aligned}$$

Table 2
Definitions of $\triangle_{ip}$, $\triangle_{i\bar{p}}$, $\triangle'_{ip}$, and $\triangle'_{i\bar{p}}$ for all k_i's

i	$\triangle_{ip}$	$\triangle_{i\bar{p}}$	$\triangle'_{ip}$	$\triangle'_{i\bar{p}}$	i	$\triangle_{ip}$	$\triangle_{i\bar{p}}$	$\triangle'_{ip}$	$\triangle'_{i\bar{p}}$
1	$\triangle(a,b,p)$	$\triangle(a,c,d)$	$\triangle(a,c,p)$	$\triangle(a,b,d)$	13	$\triangle(c,b,p)$	$\triangle(c,a,d)$	$\triangle(c,a,p)$	$\triangle(c,b,d)$
2	$''$	$\triangle(a,d,c)$	$\triangle(a,d,p)$	$\triangle(a,b,c)$	14	$''$	$\triangle(c,d,a)$	$\triangle(c,d,p)$	$\triangle(c,b,a)$
3	$\triangle(a,c,p)$	$\triangle(a,b,d)$	$\triangle(a,b,p)$	$\triangle(a,c,d)$	15	$\triangle(c,a,p)$	$\triangle(c,b,d)$	$\triangle(c,b,p)$	$\triangle(c,a,d)$
4	$''$	$\triangle(a,d,b)$	$\triangle(a,d,p)$	$\triangle(a,c,b)$	16	$''$	$\triangle(c,d,b)$	$\triangle(c,d,p)$	$\triangle(c,a,b)$
5	$\triangle(a,d,p)$	$\triangle(a,c,b)$	$\triangle(a,c,p)$	$\triangle(a,d,b)$	17	$\triangle(c,d,p)$	$\triangle(c,a,b)$	$\triangle(c,a,p)$	$\triangle(c,d,b)$
6	$''$	$\triangle(a,b,c)$	$\triangle(a,b,p)$	$\triangle(a,d,c)$	18	$''$	$\triangle(c,b,a)$	$\triangle(c,b,p)$	$\triangle(c,d,a)$
7	$\triangle(b,a,p)$	$\triangle(b,c,d)$	$\triangle(b,c,p)$	$\triangle(b,a,d)$	19	$\triangle(d,b,p)$	$\triangle(d,c,a)$	$\triangle(d,c,p)$	$\triangle(d,b,a)$
8	$''$	$\triangle(b,d,c)$	$\triangle(b,d,p)$	$\triangle(b,a,c)$	20	$''$	$\triangle(d,a,c)$	$\triangle(d,a,p)$	$\triangle(d,b,c)$
9	$\triangle(b,c,p)$	$\triangle(b,a,d)$	$\triangle(b,a,p)$	$\triangle(b,c,d)$	21	$\triangle(d,c,p)$	$\triangle(d,b,a)$	$\triangle(d,b,p)$	$\triangle(d,c,a)$
10	$''$	$\triangle(b,d,a)$	$\triangle(b,d,p)$	$\triangle(b,c,a)$	22	$''$	$\triangle(d,a,b)$	$\triangle(d,a,p)$	$\triangle(d,c,b)$
11	$\triangle(b,d,p)$	$\triangle(b,c,a)$	$\triangle(b,c,p)$	$\triangle(b,d,a)$	23	$\triangle(d,a,p)$	$\triangle(d,c,b)$	$\triangle(d,c,p)$	$\triangle(d,a,b)$
12	$''$	$\triangle(b,a,c)$	$\triangle(b,a,p)$	$\triangle(b,d,c)$	24	$''$	$\triangle(d,b,c)$	$\triangle(d,b,p)$	$\triangle(d,a,c)$

$$
\begin{aligned}
&- [(b_y - p_y)\triangle(a,c,d) + (c_y - d_y)\triangle(a,b,p)] \\
&\times \triangle(a,b,d)\triangle(a,c,p)]^2 \\
&+ [(d_y - a_y)\triangle(a,c,p)\triangle(a,b,p)\triangle(a,c,d) \\
&- (p_y - a_y)\triangle(a,c,d)\triangle(a,b,d)\triangle(a,c,p)]^2 \\
&+ [(p_y - a_y)\triangle(a,b,d)\triangle(a,b,p)\triangle(a,c,d) \\
&- (d_y - a_y)\triangle(a,b,p)\triangle(a,b,d)\triangle(a,c,p)]^2 \\
&+ [(a_y - b_y)\triangle(a,c,p)\triangle(a,b,p)\triangle(a,c,d) \\
&- (a_y - c_y)\triangle(a,b,p)\triangle(a,b,d)\triangle(a,c,p)]^2 \\
&+ [(a_y - c_y)\triangle(a,b,d)\triangle(a,b,p)\triangle(a,c,d) \\
&- (a_y - b_y)\triangle(a,c,d)\triangle(a,b,d)\triangle(a,c,p)]^2\}. \qquad (11)
\end{aligned}
$$

As can be seen in Eq. (8), the denominator part of the cross-ratio k_1 corresponds to the product of signed areas of two triangles. Let $\triangle_{1p}$ ($\triangle_{1\bar{p}}$) denote the signed area with (without) p as a vertex of the triangle, i.e., $\triangle_{1p} = \triangle(a,b,p)$ and $\triangle_{1\bar{p}} = \triangle(a,c,d)$. Similarly, in the numerator, let $\triangle'_{1p} = \triangle(a,c,p)$ and $\triangle'_{1\bar{p}} = \triangle(a,b,d)$.[5] (See Table 2 for the definitions for all k_i's.)

Accordingly, Eq. (11) can be expressed in a simpler form as

$$
\begin{aligned}
e_{k_1 x} = \frac{1}{|\triangle_{1p}|^4\ |\triangle_{1\bar{p}}|^4} &\times \{[[(b_y - d_y)\triangle'_{1p} + (c_y - p_y)\triangle'_{1\bar{p}}]\triangle_{1p}\triangle_{1\bar{p}} \\
&- [(b_y - p_y)\triangle_{1\bar{p}} + (c_y - d_y)\triangle_{1p}]\triangle'_{1\bar{p}}\triangle'_{1p}]^2 \\
&+ [(d_y - a_y)\triangle_{1p} - (p_y - a_y)\triangle'_{1\bar{p}}]^2\ (\triangle_{1\bar{p}}\triangle'_{1p})^2 \\
&+ [(p_y - a_y)\triangle_{1\bar{p}} - (d_y - a_y)\triangle'_{1p}t]^2\ (\triangle_{1p}\triangle'_{1\bar{p}})^2 \\
&+ [(a_y - b_y)\triangle_{1\bar{p}} - (a_y - c_y)\triangle'_{1\bar{p}}]^2\ (\triangle_{1p}\triangle'_{1p})^2 \\
&+ [(a_y - b_y)\triangle_{1p} - (a_y - c_y)\triangle'_{1p}]^2\ (\triangle_{1\bar{p}}\triangle'_{1\bar{p}})^2\}. \qquad (12)
\end{aligned}
$$

Expressions of similar form can also be derived for the amplification factor $e_{k_1 y}$, as well as for the amplification factors for other k_i's, $1 \leqslant i \leqslant 24$.

With the $1/(|\triangle_{1p}|^4|\triangle_{1\bar{p}}|^4)$ term in Eq. (12), it is very much likely that the k_i which has the maximum value of $|\triangle_{ip}|\ |\triangle_{i\bar{p}}|$ will have the minimum $e_{k_1 x}$ and $e_{k_1 y}$.[6] Such an observation motivates approaches proposed in the following subsections for a quick identification of minimum error amplification factors, and the corresponding cross-ratios.

4.2. Maximum denominator method

According to the geometry-based error analysis presented in the previous subsection, we now propose the

[5] The notations $\triangle_{ip}$, $\triangle_{i\bar{p}}$, $\triangle'_{ip}$ and $\triangle'_{i\bar{p}}$, which are identical to k_{ia}, k_{ib}, k_{ic} and k_{id} defined in Ref. [1], are introduced here to make easy the mathematical reasoning for proposed approaches to estimating minimum amplification factors of error variances for the cross-ratios listed in Table 1.

[6] Due to its complex computation, similar rules based on the numerator part are yet to be developed.

first algorithm, namely the maximum denominator (MD) method. The MD method identifies, for each point feature, the cross-ratio with the maximum denominator magnitude

$$k_i, i = \arg\left(\max_{1 \leqslant i \leqslant 24} |\triangle_{ip}|\ |\triangle_{i\bar{p}}|\right) \tag{13}$$

as the one with the smallest error amplification factors $e_{k_i x}$ and $e_{k_i y}$. (Assume $\sigma_{xx}^2 = \sigma_{yy}^2$, the minimization of $e_{k_i x} + e_{k_i y}$ is considered.) In fact, it is not necessary to check all 24 cross-ratios since, as one can see from the third and the last column (dependency) of Table 1, they can be divided into pairs of cross-ratios with each pair having identical behavior in error amplification; hence, only 12 cross-ratios are to be examined. Thus, for each point feature under consideration, the cross-ratio with minimum error amplification factors is identified by the following procedure (assuming that only odd i's are taken into account).

The MD procedure:

Step 1. Identify the cross-ratio

$$k_i, i = \arg\left(\max_{1 \leqslant i \leqslant 12} |\triangle_{(2i-1)p}|\ |\triangle_{(2i-1)\bar{p}}|\right) \tag{14}$$

as the one with smallest error amplification factors $e_{k_i x}$ and $e_{k_i y}$.

For some situations which are not uncommon, on the other hand, we can consider $|\triangle_{ip}|$'s and $|\triangle_{i\bar{p}}|$'s separately for more efficient computation, as will be discussed next.

4.3. Two-step method $|\triangle_{ip}|$ then $|\triangle_{i\bar{p}}|$

To accelerate the estimation of error amplification factors based on Eq. (14), the second method, namely the two-step (TS) method, is developed based on the following observations. Consider the 12 $|\triangle_{ip}|\ |\triangle_{i\bar{p}}|$'s in Eq. (14) calculated for each feature point. If the four reference points are selected in advance, the $|\triangle_{i\bar{p}}|$'s will be fixed. Furthermore, the $|\triangle_{i\bar{p}}|$'s will not be very different from one another if locations of the reference points are chosen properly, e.g., the points are distributed fairly symmetrically with respect to their centroid. On the other hand, the $|\triangle_{ip}|$'s may vary significantly because, in principle, a feature point p can appear in any location in an image. The above observations suggest that the identification of the maximum denominator may be achieved approximately by evaluating $|\triangle_{ip}|$'s first and then $|\triangle_{i\bar{p}}|$'s.

According to the properties of the triangle function, defined in Eq. (7), only six different $|\triangle_{ip}|$'s, each representing two cross-ratios, need to be considered. For example, we have $|\triangle_{1p}| = |\triangle_{7p}|$ for k_1 and k_7 from Table 2. Accordingly, the TS method first calculates six different values of $|\triangle_{ip}|$ and identifies two of the 12 cross-ratios having the maximum $|\triangle_{ip}|$. Subsequently, one of the two cross-ratios which has larger $|\triangle_{ip}|\ |\triangle_{i\bar{p}}|$ is identified as the one with minimum error amplification factors. In summary, we have the following procedure to identify the cross-ratio with minimum error amplification factors.

The TS procedure:

Step 1. Calculate the six $|\triangle_{ip}|$'s, i.e., for $i = 1, 3, 5, 9, 11$ and 17.

Step 2. For the maximum $|\triangle_{ip}|$ obtained in Step 1, identify the cross-ratio

$$k_i, i = \arg\left(\max_{\substack{i \neq j \\ |\triangle_{ip}| = |\triangle_{jp}|}} (|\triangle_{i\bar{p}}|, |\triangle_{j\bar{p}}|)\right) \tag{15}$$

as the one with smallest error amplification factors $e_{k_i x}$ and $e_{k_i y}$.

Consider the time complexity of the three methods. The $|\theta - 90^\circ|$ criterion suggested in Ref. [1] requires the computation of 12 θ's for comparison. Simplification of the estimation is possible by considering the value of

$$\cos^2\theta = \left(\frac{\mathbf{oo}' \cdot \mathbf{op}}{|\mathbf{oo}'|\ |\mathbf{op}|}\right)^2. \tag{16}$$

Thus, a total of 68 multiplication and 12 division operations is required. On the other hand, the MD method requires the evaluation of 12 cross-ratio denominators, which involve the calculation of $\binom{5}{3} = 10$ cross-products, or 20 multiplication operations equivalently, to find $|\triangle_p|$'s and $|\triangle_{\bar{p}}|$'s, and additional 12 multiplication operations to find the 12 $|\triangle_p|\ |\triangle_{\bar{p}}|$'s. Finally, the TS method checks 6 cross products in the first step, and then 2 more in the second, which require a total of 16 multiplication operations.

5. Simulation results

This section reports the simulation results obtained with estimation methods, MD and TS, proposed in the previous section, as well as the method suggested in Ref. [1], denoted here as *orthogonal method* (OR). Two simulations are provided to examine their performances under different conditions. Fig. 3 shows a 500×500 image of reference points used in the two simulations. While $\{a, b, c_1, d\}$, representing a typical geometry of reference points, are used in the first simulation, point c_1 is replaced with c_2 in the second simulation in which three of the reference points are nearly collinear.

5.1. Simulation 1 — a typical situation

In this simulation, locations of the four reference points, $a = (109, 112)$, $b = (96, 285)$, $c_1 = (365, 390)$ and $d = (312, 227)$, are assumed to be identical to that shown in fig. Fig. 6 of Ref. [1]. The error variance is considered for the projective coordinates of feature points p_i's located on a regular grid of size $21 \times 21 = 441$. For example, $p_1 = (0, 0), p_2 = (0, 25)$, and so on.

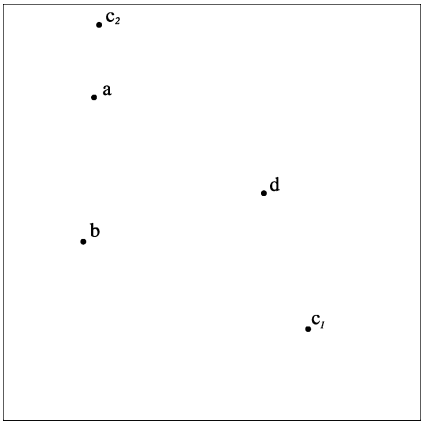

Fig. 3. The 500×500 image of reference points used in the two experiments.

For simplicity, assume that $\sigma_{xx}^2 = \sigma_{yy}^2 = 1$ and $\sigma_{xy} \cong 0$. The error variances of k_i, similar to that formulated in Eq. (9) for k_1, can be expressed as

$$\sigma_{k_i,k_i}^2 = e_{k_i x} + e_{k_i y}. \tag{17}$$

Accordingly, the 12 error variances, $\sigma_{k_{2i-1}k_{2i-1}}^2$, $1 \leqslant i \leqslant 12$, can be calculated and the minimum error variance, denoted as σ_m^2, can be identified for each feature point.

Without carrying out the complex calculation of all 12 variances, the three estimation methods (MD, TS and OR) are applied, respectively, to choose a k_i which is supposed to have the minimum $\sigma_{k_i k_i}^2$ for each feature point. Fig. 4 shows the minimum $\sigma_{k_i k_i}^2$ estimated by the above three methods, denoted as $\sigma_{m,\mathrm{MD}}^2$, $\sigma_{m,\mathrm{TS}}^2$ and $\sigma_{m,\mathrm{OR}}^2$, respectively, for the 441 feature points. One can see clearly that while MD and TS methods both yield low error variances with hardly noticeable differences, the minimum error variances estimated by the OR method are significantly higher. For example, a peak can be observed for the OR method for $p_{283} = (325, 225)$, which is located very close to d. Since $\angle c_1\,\mathrm{d}p$ is the closest to 90°, k_{22} with a very small $\triangle_{ip} = \triangle \mathrm{d}c_1 p$ is chosen according to the $|\theta - 90^\circ|$ criterion, resulting in a large error variance. Similar explanations can be given for peaks associated with p_{98}, p_{97}, etc., obtained from the OR method.

Such a performance difference could be explained partly as follows. For any 2D feature point p, the error variances associated with the 12 k_i's depend on the coordinates of four reference points and that of p itself, i.e., there are ten variables ($a_x, a_y, \ldots, d_x, d_y$ and p_x, p_y) which need to be considered. Without an obvious mathematical support, the $|\theta - 90^\circ|$ criterion adopted in the OR method can hardly capture the complex effects due to so many variables. On the other hand, the denominator part of cross-ratio adopted in the proposed methods exhibits itself as a reasonable and efficient indication of the relative magnitude of error variances expressed in Eq. (9).

From another perspective, the above results can also be demonstrated directly on the image plane. As the basis for performance comparison, Fig. 5(a) shows the 21×21 minimum error variance σ_m^2 obtained through direct calculation, e.g., using Eq. (9) for k_1. The gray value is made to vary logarithmically with the darkest (brightest) gray level denoting the value of 10^{-5} ($10^{-3.8}$). Similarly, Fig. 5((b)–(d)), show the differences, $\sigma_{m,\mathrm{OR}}^2 - \sigma_m^2$, $\sigma_{m,\mathrm{MD}}^2 - \sigma_m^2$ and $\sigma_{m,\mathrm{TS}}^2 - \sigma_m^2$, respectively, with the darkest (brightest) gray level denoting the difference of 10^{-7} (10^{-2}). It is readily observable from these differ-

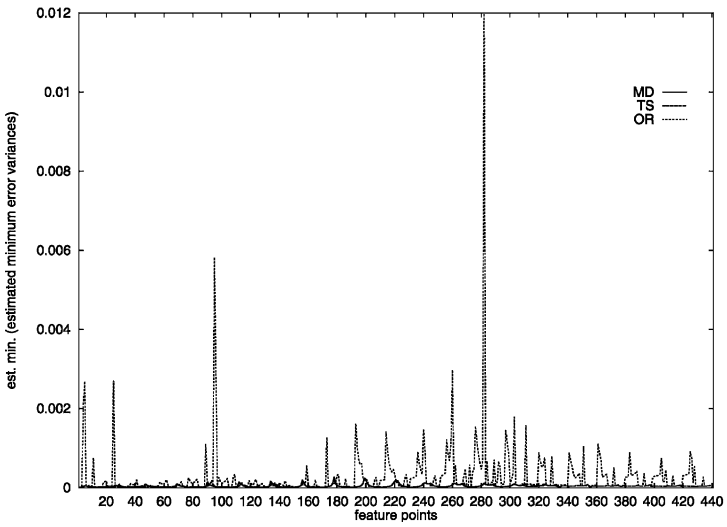

Fig. 4. The minimum $\sigma_{k_i k_i}^2$ estimated by the three estimation methods for the 441 feature points.

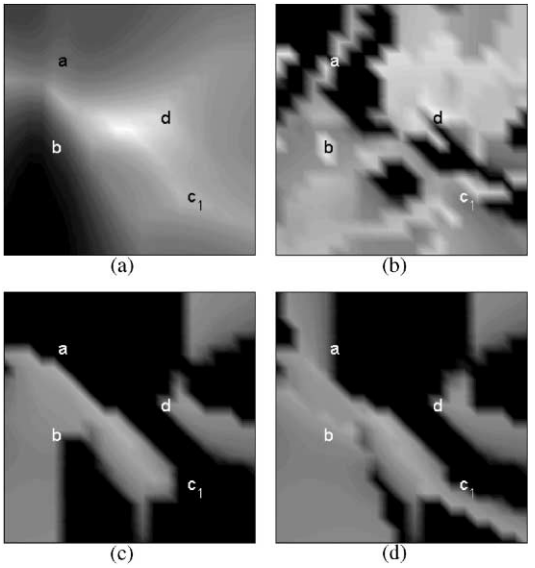

Fig. 5. Gray-level images representing the minimum error variances and the differences between these minimum and those obtained with OR, MD and TS methods, respectively. (a) σ_m^2, (b) $\sigma_{m,\mathrm{OR}}^2 - \sigma_m^2$, (c) $\sigma_{m,\mathrm{MD}}^2 - \sigma_m^2$, (d) $\sigma_{m,\mathrm{TS}}^2 - \sigma_m^2$.

ences that (i) the deviations from σ_m^2 are much higher for the OR method than the other two, and (ii) the MD and TS methods have very similar behaviors in estimating σ_m^2 in terms of the magnitude of estimation error as well as the distribution of such error in different image locations. While (i) is consistent with the results shown in Fig. 4, (ii) is due to the fact that, in principle, the TS method is a simplification of the MD method with minor modifications.

In general, for each feature point, besides the k_i with the smallest error variance (σ_m^2), those with slightly higher error variances may also be used as projective coordinates to generate satisfactory reconstruction results. Fig. 6 shows for each of the three estimation approaches, the total number of the 21×21 locations for which the cross-ratio with the smallest (black), the second smallest (gray) and the third smallest (white) error variances will be selected. While the MD method results in good estimates for most locations, the OR results correspond to the least, as expected.

To investigate the behavior of the OR method further, a special configuration of reference points will be considered in the following example. Such an example also partly addresses the issue of the selection between the MD and TS methods under different conditions.

5.2. Simulation 2 — a special case

In Fig. 3, consider the set of reference points which is slightly different from those used in Simulation 1 in that

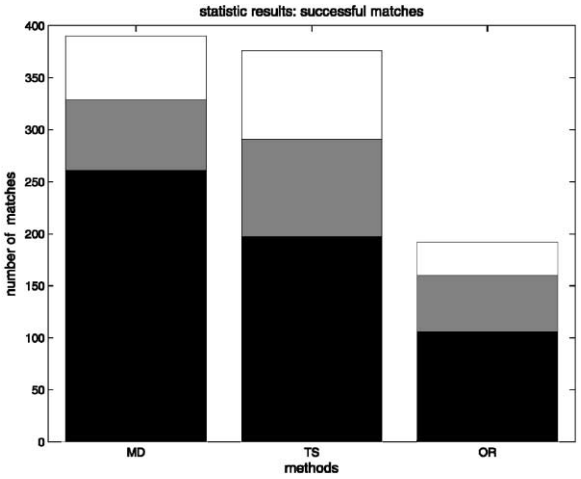

Fig. 6. The total number of the 21×21 locations for which the cross-ratio with the smallest (black), the second smallest (gray) and the third smallest (white) error variances will be selected.

c_1 is replaced with c_2.The situation corresponds to a special configuration of the reference points, i.e., a, b and c_2, are near-collinear in the projective image. Figs. 7 and 8 show simulation results similar to Figs. 4 and 5, respectively, obtained in Simulation 1. The error variances in Fig. 7 are shown in logarithmic scale to accommodate dramatically increased dynamic range of the error variances obtained with the OR method. Notice that extremely large error variance values occur for a subset of the first 170 feature points. On the other hand, the dynamic ranges for the MD and TS methods seem to be similar to that shown in Fig. 4. In Fig. 8(a), the minimum error variances are shown to have a different distribution of overall increased values due to the change of the configuration of the reference points. For the results shown in Figs. 8(b)–(d), observations similar to that for Figs. 5(b)–(d) can be obtained except for (i) the extremely large values resulting from the OR method (as mentioned earlier), and (ii) a bigger difference between the MD and TS methods compared with the results shown in Fig. 5.

For a more in-depth analysis of (i), Fig. 9 extracts the error amplification zone ($\sigma_{m,\mathrm{OR}}^2 \geqslant 1$) from Fig. 8(b) and shows the cross-ratio, explicitly by its index, chosen by the OR method at each grid location in the zone. Clearly, the zone can be divided into three parts. For example, for the darkest (black) area shown in Fig. 9, which includes a region near the line passing through point b and perpendicular to $\overline{bd}$, $\angle dbp$ is the closest to 90° compared to the other 11 θ's; hence, according to the OR estimation, k_{11} or k_{12} will be selected.[7] However, the two cross-

[7] In theory, the cosine function given in Eq. (16) will yield the same magnitude for both k_{11} and k_{12}. Hence, the selection between the two is simply a consequence of numerical differences.

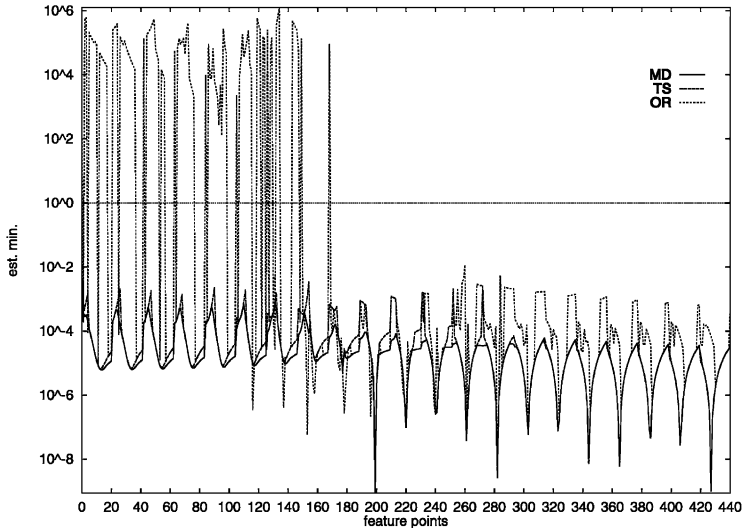

Fig. 7. The minimum $\sigma^2_{k_i k_l}$ similar to Fig. 4, estimated by the three estimating methods for the 441 feature points, for simulation 2.

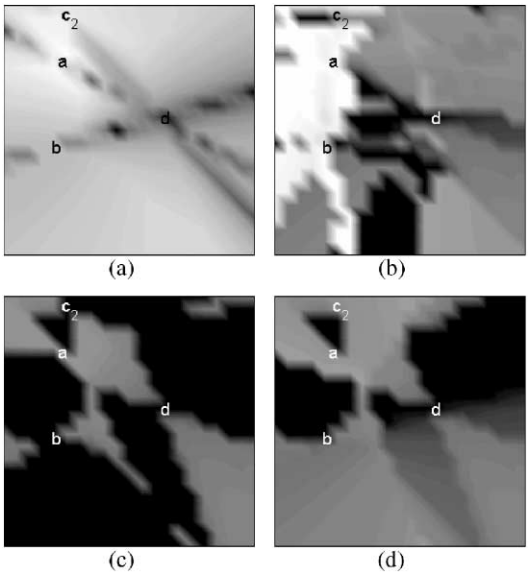

Fig. 8. Gray-level images, similar to those shown in Fig. 5, obtained for simulation 2. (a) σ^2_m, (b) $\sigma^2_{m,\mathrm{OR}} - \sigma^2_m$, (c) $\sigma^2_{m,\mathrm{MD}} - \sigma^2_m$, (d) $\sigma^2_{m,\mathrm{TS}} - \sigma^2_m$.

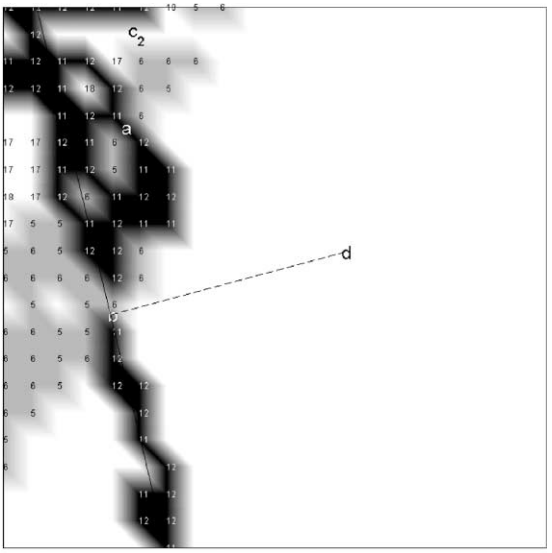

Fig. 9 . The cross-ratio chosen by the OR method, at each grid location in the error amplification zone.

ratios correspond to the worst choices. This is because their denominators also contain a $\triangle_{i\bar{p}}$ ($\triangle(b,c,a)$ or $\triangle(b,a,c)$, see Table 2) with extremely small magnitudes due to the near collinearity, resulting in unacceptably large error variances. Similar observations can be made for other feature points shown in Fig. 9 which are located near the line passing through point $a(c_2)$ and perpendicular to $\overline{ad}(\overline{c_2 d})$ for which cross-ratio k_5 or k_6 (k_{17} or k_{18}) will be selected. In contrast, since both $|\triangle_p|$ and $|\triangle_{\bar{p}}|$ are considered, an extremely large σ^2_m does not appear in the MD or the TS results. For example, for the TS method, we have $\max\{|\triangle_p|\} = |\triangle(b,d,p_1)| = |\triangle(d,b,p_1)|$ for p_1; however, since $|\triangle(b,c_2,a)| \cong 0$, the TS method will choose $\triangle_p = \triangle(d,b,p_1)$. Therefore, either k_{19} or k_{20} will be selected.

The reason for (ii) is that, while the MD method takes into account 12 $|\triangle_p|$ $|\triangle_{\bar{p}}|$'s, the TS method considers only 6 $|\triangle_p|$'s and then proceeds with the estimation only for the $\max\{|\triangle_p|\}$. It is easy to see that such a strategy

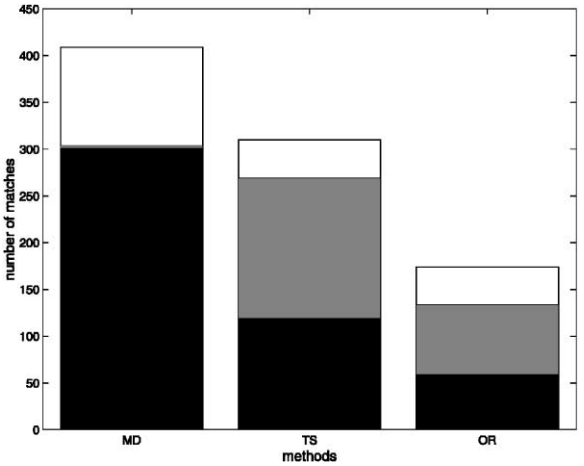

Fig. 10. Simulation results, similar to that shown in Fig. 6, obtained for simulation 2.

will reduce the overall searching space and, somehow in the special case considered in Simulation 2, results in a larger performance difference between the two methods. Fig. 10 shows the results similar to that shown in Fig. 6. If one only considers $\sigma^2_{m,\mathrm{MD}}$ and $\sigma^2_{m,\mathrm{TS}}$ (black areas), an improvement of the MD results as well as a degeneration of the TS results can be seen clearly. Even so, on the grounds that both $\sigma^2_{m,\mathrm{MD}}$ and $\sigma^2_{m,\mathrm{TS}}$ do not exceed 10^{-2} at all times, as shown in Fig. 7, both methods are considered as generating satisfactory results. Nevertheless, deciding whether the MD or the TS method should be adopted under different conditions is not trivial in general and requires further investigations.

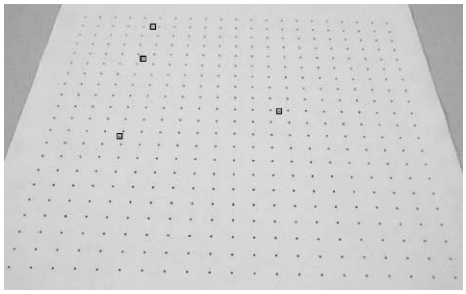

Fig. 11. A 642×1024 image of the 21×21 grid points and the four reference points marked with squares.

5.3. Experiments using real images

In our work, experiments using real images are carried out to verify the simulations performed in the previous subsections. For brevity, only the experiments for Simulation 2 are presented in this subsection. Fig. 11 shows a 642×1024 image of the 21×21 grid points and the four reference points marked with squares. Locations of all these points with image pixel precision are obtained with ordinary point detection algorithm.

For each grid point, cross-ratios which are identified in the previous subsection to have $\sigma^2_{m,\mathrm{MD}}$, $\sigma^2_{m,\mathrm{TS}}$, $\sigma^2_{m,\mathrm{OR}}$, respectively, are calculated. Fig. 12 shows errors in these cross-ratio values compared with their theoretical values for all the grid points. It is readily observable that the errors are fairly consistent with the statistical results shown in Fig. 7. Similar results, which are not included here for brevity, are also obtained for images of the same scene taken from other viewpoints.

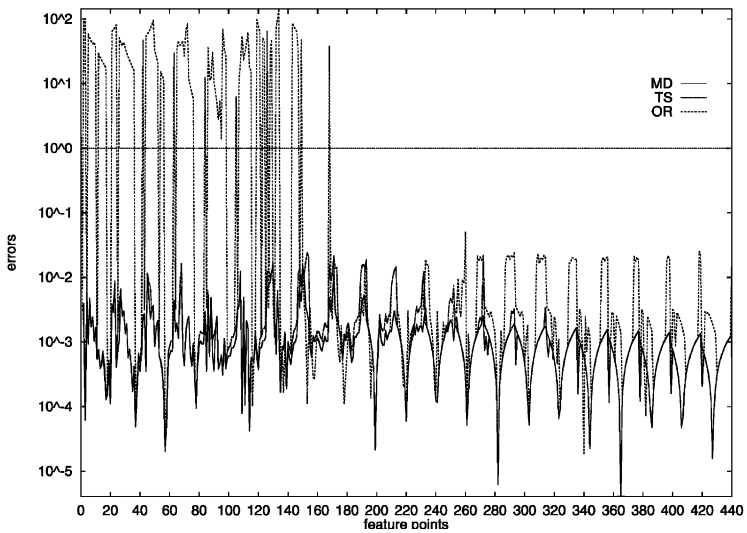

Fig. 12 . Errors in values of cross-ratios corresponding to $\sigma^2_{m,\mathrm{MD}}, \sigma^2_{m,\mathrm{TS}}, \sigma^2_{m,\mathrm{OR}}$, respectively, calculated for the images of the 441 grid points shown in Fig. 11.

6. Summary

This paper concerns error analysis for perspective projection-based 3D shape reconstruction. Based on a normal distribution assumption, formulation of error variances for different cross-ratios with respect to a set of reference points utilized in the reconstruction is established. According to a geometry-based mathematical reasoning, the proposed error estimation approach suggests that the cross-ratios with the maximum denominator magnitudes, i.e., the maximum products of areas of two corresponding triangles, will lead to the minimum amplifications of error variance. Subsequently, the MD procedure for error estimation is developed. Compared with the OR method suggested in Ref. [1], the proposed approach generates better results for an ordinary configuration of four reference points as well as for a special one. In the latter case, three reference points are nearly collinear. A brief explanation is also given for the significantly worse results obtained with the estimation method presented in Ref. [1] for such a special case.

As an alternative to the MD method which already requires less computation than the OR method, the more efficient TS method is also introduced. The latter is a straightforward simplification of the former which considers the area of one triangle, instead of the product of two triangles, at a time and effectively halves the computation costs. However, as for the trade-off between the two methods, it is not trivial to decide whether the MD or the TS method should be adopted under different conditions, and this requires further investigations.

References

[1] N. Georis, M. Petrou, J. Kittler, Error guided design of a 3D vision system, IEEE Trans. Pattern Anal. Mach. Intell. 20 (4) (1998) 366–379.
[2] C. Slama (Ed.), The manual of photogrammetry, The American Society of Photogrammetry, Falls Church, VA 22046, 1980.
[3] E. Mikhail, Observations and Least Squares, IEP — A Dun-Donnelley Publisher, New York, 1976.
[4] K.R. Koch, Parameter estimation and hypothesis testing in Linear Models, Springer, Berlin, 1987.
[5] R.M. Haralick, Propagating covariance in computer vision, Proceedings of the 12th IAPR, Jerusalem, Israel, 9–13 October, IEEE CS Press, Los Alamitos, CA, 1994, pp. 493–498.
[6] R.Y. Tsai, A versatile camera calibration technique for high-accuracy 3D machine vision metrology using off-the-shelf TV cameras and lenses, IEEE J. Robot. Automat. 3 (4) (1987) 323–344.
[7] A. Cumani, A. Guiducci, A new camera calibration method for high accuracy non-contact metrology, Pattern Recognition Lett. 14 (1993) 415–419.
[8] Z.Q. Hong, J.Y. Yang, An algorithm for camera calibration using a three-dimensional reference point, Pattern Recognition 26 (1993) 1655–1660.
[9] J.J. Koenderink, A.J. van Doorn, Affine structure from motion, Tech. Rep., Utrecht University, Utrecht, The Netherlands, October 1989.
[10] A. Shashua, Projective structure from uncalibrated images: structure from motion and recognition, IEEE Trans. Pattern Anal. Mach. Intell. 16 (8) (1994) 778–790.
[11] A. Shashua, N. Navab, Relative affine structure: theory and application to 3D reconstruction from perspective views, IEEE Trans. Pattern Anal. Mach. Intell. 18 (9) (1996) 873–883.
[12] R. Mohr, L. Morin, Relative positioning from geometric invariants, Proceedings of the Conference of Computer Vision and Pattern Recognition, 1991 pp. 134–144.
[13] R. Mohr, E. Arbogast, It can be done without camera calibration, Pattern Recognition Lett. 12 (1991) 39–43.
[14] S. Carlsson, Projectively invariant decomposition and recognition of planar shapes, Proceedings of the International Conference of Computer Vision, 1993, pp. 471–475.
[15] H. Chabbi, M. Berger, Recovering Planar Surfaces by Stereo Vision Based on Projective Geometry, Tech. Rep. 93-R-054, CRIN/CNRS-INRIA, Lorraine, 1993.
[16] R.T. Collins, R.J. Beveridge, Matching perspective views of coplanar structures using projective unwarping and similarity matching, Proceedings of the Conference of Computer Vision and Pattern Recognition, New York, IEEE CS Press, Los Alamitos, CA, June 1993, pp. 240–245.
[17] O.D. Faugeras, What can be seen in three dimension with an uncalibrated stereo rig?, Proceedings of the Second European Conference of Computer Vision, Santa Margherita Ligure, Italy, May 1992, pp. 563–578.
[18] S.J. Maybank, Probabilistic analysis of the application of the cross ratio to model based vision: misclassifcation, Int. J. Computer Vision 14 (1995) 199–210.
[19] S.J. Maybank, Probabilistic analysis of the application of the cross ratio to model based vision, Int. J. Computer Vision 16 (1995) 5–33.
[20] N. Efimov, Advanced Geometry, MIT, Moscow, 1978.
[21] R. Mohr, Projective geometry and computer vision, Handbook Pattern Recognition Comput. Vision, (1993) 269–293.

About the Author—JAIN-SHING LIU was born in Taipei, Taiwan, in 1970. Currently, he is working toward the Ph.D. degree in Department of Computer and Information Science, National Chiao Tung University, Hsinchu, Taiwan. His current research interests include 3-D modeling, computer vision and image processing.

About the Author—JEN-HUI CHUANG (S'86–M'91) received the B.S. degree in electrical engineering from National Taiwan University, Taipei, Taiwan, ROC, in 1980, the M.S. degree in electrical and computer engineering from the University of California at

Santa Barbara in 1983, and the Ph.D. degree in electrical and computer engineering from the University of Illinois at Urbana-Champaign in 1991.

Between 1983 and 1985, he was a Design and Development Engineer with the LSI Logic Corporation, Milpitas, CA. Between 1989 and 1991, he was a Research Assistant with the Robot Vision Laboratory, Beckman Institute for Advanced Science and Technology, University of Illinois, Champaign, IL. Since August 1991, he has been on the faculty of the Department of Computer and Information Science, National Chiao Tung University, Hsinchu, Taiwan. His research interests include 3-D modeling, computer vision, speech and image processing and VLSI systems.

Dr. Chuang is a Member of the Tau Beta Pi Society.